DEHYDROGENATION IN ELECTRON-INDUCED DISSOCIATIVE IONIZATION OF PYRIDINE MOLECULE

MICHAL K. JURKOWSKI, TOMASZ J. WASOWICZ*

Division of Complex Systems Spectroscopy, Institute of Physics and Computer Science, Gdansk University of Technology, ul. G. Narutowicza 11/12, 80-233 Gdansk, Poland
* *E-mail*: tomasz.wasowicz1@pg.edu.pl

Received May 17, 2023

Abstract. The electron-impact dissociative ionization of pyridine has been investigated using mass spectrometry. Thirty-two well-resolved mass peaks have been identified in the cation mass spectra and assigned to the most likely ionic molecular fragments. The new sixteen ionic fragments' appearance energies have been determined, and sixteen others remeasured. The total cross-section for electron-impact ionization of pyridine has been measured at 100 eV. Thorough analysis indicates that at least three peaks' groups in the mass spectra occur *via* the shake-off dehydrogenation mechanism, *i.e.*, by sequential hydrogen atoms elimination from the pyridine parent cation or its fragmentation products. The nature of this process is deciphered.

Key words: Pyridine, shake-off dehydrogenation, ThreSpect, cross-section, thresholds, dissociation, ionization, mass spectra, electrons.

DOI: https://doi.org/10.59277/RomJPhys.2023.68.205

1. INTRODUCTION

Heterocyclic molecules are ubiquitous. Their rings are incorporated in technological and naturally occurring chemical compounds, such as synthetic and natural dyes, nucleic acids, most drugs, vitamins, etc. They are often exposed to various forms of radiation in natural environments or during engineering or medical processes. Therefore, their interactions with photons [1–8], electrons [9–12], and ions [13–21] have been recently investigated.

In particular, pyridine (C_5H_5N) is a model bioactive six-membered nitrogen-containing heterocycle compound with many biological, pharmaceutical, and agrochemical applications [22]. It is incorporated into B vitamins [22], coenzymes, and alkaloids [23]. Since the discovery of pyridine derivatives: niacin, pyrimidines, and purines in carbonaceous chondrites [24, 25], traces of pyridine as a precursor of the building block of biologically active molecules have been incessantly sought in the interstellar media [26]. Pyridine can thus be found under a variety of irradiation conditions, and many studies have recently probed its absorption, excitation, ionization, and fragmentation (see, *e.g.*, [26–36]) to understand its response to different radiation forms.

The possibility of hydrogen atoms detaching from the pyridine ring has been observed among various decomposition routes. However, any study has shown the

possibility of successive shake-off dehydrogenation of its ring or major fragments. Therefore in the present work, we have studied the electron-impact dissociative ionization of pyridine with a focus on the dehydrogenation of the pyridine parent cation or its fragmentation products.

2. EXPERIMENTAL DETAILS

The electron impact mass spectrometry (EIMS) experiment was performed using an EPIC 300 (Hiden Analytical Ltd.) quadrupole mass spectrometer at the Laboratory of Complex Systems Spectroscopy (Fahrenheit Universities' core lab) of the Gdansk University of Technology. This setup has been presented in detail previously (*e.g.*, [37]), and only a brief description combined with pyridine specifics is given here.

The mass spectrometer consisted of an internal electron impact ionization source, the ion extractor, focusing, and energy filter aperture electrodes mounted before the quadrupole mass filter, followed by a secondary electron multiplier as an ion detector. The cage connected to the positive voltages surrounded the ionization region in the electron ionizer. The incident electron beam current in the ionizer was usually 0.3 or 30 μA. The extracted electrons collided with the effusive beam of pyridine introduced into the interaction region by a narrow stainless steel capillary installed 5 mm from the ionization cage. As a result of this interaction, the pyridine is ionized and fragmented. The focusing electrode was maintained at a higher negative voltage of −200 V to adjust the arising cations' optimal transmission efficiency. A 70 l/s turbomolecular pump pumped the spectrometer's vacuum chamber to a 10^{-8} mbar base pressure. After introducing the pyridine vapors, the operating pressure in the collision chamber was set at $1{-}3 \times 10^{-6}$ mbar. We confirmed linear dependence between the detected cation signal and the incident electron current with operating pressure up to 6×10^{-6} mbar, thus suggesting a single collision regime.

The liquid pyridine (C_5H_5N) with a purity of 99.8% was procured from Sigma Aldrich, Poland. The measurements were performed at room temperature since pyridine has relatively high vapor pressure, ca. 26.7 hPa at 25°C [38]. However, the spectrometer's vacuum chamber, pipes, and valves were slightly heated to avoid sample condensation. Pyridine was degassed several times under a vacuum to eliminate vaporous contaminations in a stainless steel container before any measurements were implemented.

3. RESULTS AND DISCUSSION

In the first step of the investigations, the cationic products of the electron-impact dissociative ionization of pyridine have been identified. For that purpose,

the mass spectra were recorded in the 10–90 u mass range for fixed electron energies. By cutting off the pyridine vapor, the background signal was measured and then subtracted from mass spectra. Earlier measurements showed [37] that the transmission of this spectrometer was practically independent of the cation mass in the 10−120 u mass range.

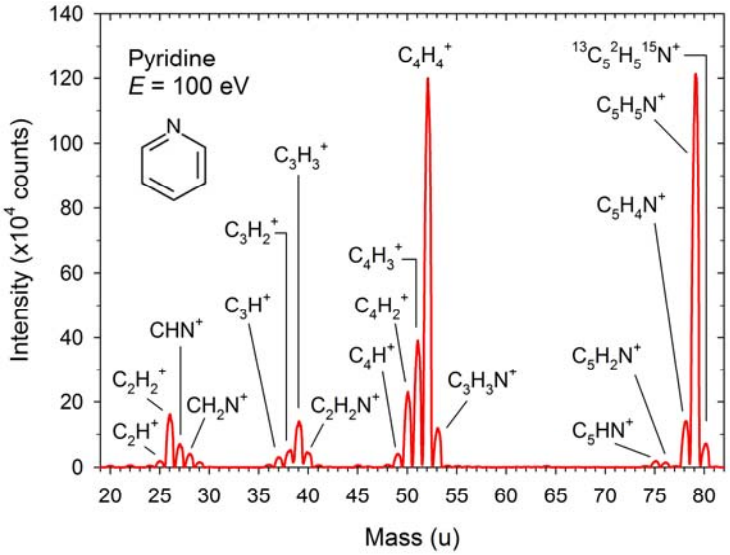

Fig. 1 – The mass spectrum of the cations of pyridine obtained at an electron energy of 100 eV.

The mass spectrum of the pyridine cations obtained at an electron energy of 100 eV is displayed in Fig. 1, together with the assignments of the mass peaks performed by Jiao *et al.* [32], who discriminated the possible isobar cations by comparing the mass spectra of pyridine and pyridine-*d*5. The present mass spectrum agrees with that published in photodissociation studies [31, 39], and the NIST database [40]. In all these spectra, the mass peaks form four groups separated well from each other on the mass scale. However, our spectrum has a higher resolution. Indeed in the present measurements, the mass resolution of the spectrometer was better than one Dalton (u), as deduced from the measured spectra. In-depth examinations of the present spectra demonstrate at m/q = 60–64 a group of very weak peaks with decreasing intensities (see Fig. 2) that arise from the dehydrogenation of the pyridine cations. Actually, each peak group has cationic fragments formed by successive hydrogen atoms abstractions (see Figs. 1 and 2).

In the second part of this work, the absolute total electron ionization cross-sections of pyridine were determined at 100 eV. We used the relative flow technique [41] based on the comparison performed under identical experimental conditions of the studied products' intensities with well-known cross-sections of standard species to obtain the absolute values. We used the 2.51×10^{-16} cm^2 value [42] measured

for Ar^+ from Ar at 100 eV as a standard cross-section. However, we employed two approaches to determine the absolute values of pyridine cross-sections.

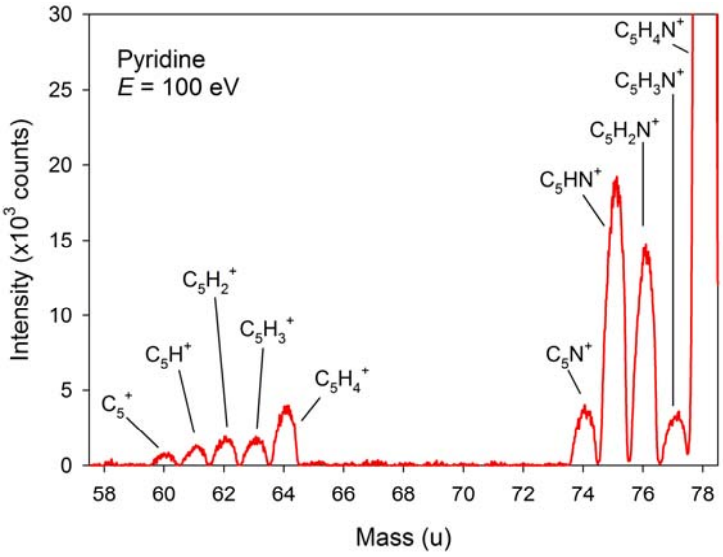

Fig. 2 – The mass peaks demonstrating dehydrogenation of the pyridine cations.

At first, the electron beam energy was kept constant at 100 eV. At this energy, we measured the intensities of the parent cation of pyridine (m/q = 79) and Ar^+ (m/q = 40) in the same experimental conditions (the same pressure, electron beam current, and recording time) and applied the formula given by Rahman and Krishnakumar [41] to obtain the cross sections. To be sure that the transmission of the spectrometer does not alter the obtained results, we repeated this procedure for the m/q = 39 pyridine cation.

In the second procedure, we maintained several pressures of the parent cation of pyridine and Ar^+ in the range of $6 \times 10^{-7} - 5 \times 10^{-6}$ mbar at constant electron beam energy (100 eV). The intensities were measured several times for different currents and recording times for each such pressure. Then the normalized intensities *versus* pressures graphs were plotted for the pyridine and the Ar targets. These graphs were linear in the studied pressure region, indicating that molecular flow had been achieved during measurements. Directly comparing these lines' slopes gave the relative levels of the cross sections [43]. The errors in this method combine the uncertainties in the Ar^+ absolute cross-section determination [42], present experimental errors, and the computed errors involved in linear regression. Knowing the other fragments' intensities (from the mass spectrum measured at 100 eV) relative to the total intensity allowed each cation to be put on an absolute scale in both procedures.

Comparing the results of these two methods indicates that within the limits of the uncertainties, both procedures give consistent cross-sections. The weighted mean

value of the total ionization cross-section of pyridine at 100 eV was found to be $(26.6 \pm 0.5) \times 10^{-17}$ cm^2. Initially, we were confounded because our result was six times lower than the cross-section measured by Jiao *et al.* [32]. However, our procedures differed from those performed by Jiao *et al.* [32]. Our ones were probably too simple and did not consider all the parameters that could affect the measurement. On the contrary, Jiao studied a mixture of pyridine and Ar using stored waveform inverse Fourier transform equipped with the cooling period that thermalized excited Ar ions and exhausted the ions with reaction rates higher than the ground state. They also eliminated the space charge effect to reduce overpopulated Ar^+ ions.

Therefore during the cross-section curves' determinations, we focused on measurements close to thresholds to determine all identified cations' appearance energies (E_{TH}). These appearance energies were obtained by fitting a modified Wannier function [44] describing the cross-sections in the near-threshold region using the "ThreSpect" software [45] downloaded from the Gdansk University of Technology Bridge of Knowledge repository [46].

The found energy shift between the E_{TH} and the spectroscopic value of the ionization energy in Ar^+ (15.76 (0.01) eV [47]) was used to calibrate the energy scale in each cross-section measurement. In addition, the energy dispersion distribution was estimated to be 600 meV from the Ar^+ yield measured just above E_{TH}.

The example patterns of such curves measured in narrow energy regions around the expected positions of the thresholds are shown in Fig. 3. The extracted E_{TH} of the thirty-two cation fragments and their uncertainties are given in Table 1. The results from other works are for comparison listed in the last column of Table 1. One can notice that our values generally are in agreement with previous studies. In addition, sixteen thresholds are determined here for the first time. These E_{TH} values were predominantly found for the lightest fragments as well as the cations formed in the sequential dehydrogenation of $C_5H_5N^+$ and $C_5H_4^+$ molecules.

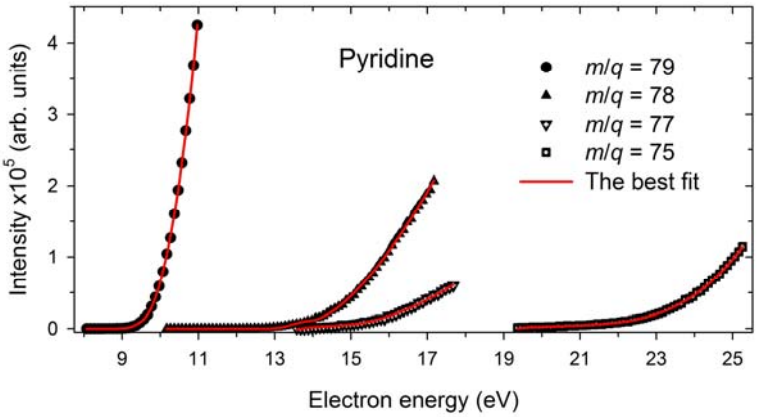

Fig. 3 – The cross-section curves measured in narrow energy regions near the expected thresholds. The solid lines represent the best fittings to the experimental points.

Table 1

Cataion assignment, threshold energies (E_{TH}), together with their uncertainties obtained for the pyridine molecules. *Both isobar ions have comparable intensities [32]

Mass [u]	Cation assignment	E_{TH} [eV]	E_{TH} [eV] literature values
12	C^+	22.3 (0.1)	
13	CH^+	32.6 (0.1)	
24	C_2^+	23.5 (0.1)	
25	C_2H^+	29.3 (0.1)	29.7 [39]
26	$C_2H_2^+$	17.4 (0.3)	16.7 [39]
27	$^*C_2H_3^+/CHN^+$	19.1 (0.1)	17.2 [39]
29	$C_2H_5^+/CH_3N^+$	13.5 (0.1)	17.2 [39]
36	C_3^+	36.1 (0.3)	
37	C_3H^+	18.2 (0.1)	27.7 [39]
38	$^*C_2N^+/C_3H_2^+$	14.4 (0.1)	23.2 [39]
39	$C_3H_3^+$	12.2 (0.1)	13.2 [39], 14.0 [48], 14.0 [49]
40	$C_2H_2N^+$	16.0 (0.1)	23.7 [39]
41	$C_3H_5^+/C_2H_3N^+$	13.3 (0.1)	
48	C_4^+	32.3 (0.4)	
49	C_4H^+	27.7 (0.2)	
50	$C_4H_2^+$	15.7 (0.2)	15.7 [39], 16.17 [48]
51	$C_4H_3^+$	15.6 (0.1)	15.7 [39], 16.61 [48]
52	$C_4H_4^+$	12.2 (0.2)	12.2 [39], 13.6 [48], 12.2 [50], 11.84 [51], 12.15 [52], 12.34 [53]
53	$C_3H_3N^+$	11.9 (0.4)	12.7 [39], 13.84 [48]
54	$C_3H_4N^+$	13.9 (0.1)	
60	C_5^+	36.7 (0.6)	
61	C_5H^+	33.4 (0.2)	
62	$C_5H_2^+$	26.3 (0.3)	
63	$C_5H_3^+$	15.9 (0.5)	
64	$C_5H_4^+$	14.9 (0.2)	
74	C_5N^+	29.8 (0.6)	
75	C_5HN^+	20.7 (0.2)	
76	$C_5H_2N^+$	16.2 (0.1)	
77	$C_5H_3N^+$	15.0 (0.1)	12.42 [48]
78	$C_5H_4N^+$	14.0 (0.1)	13.7 [39], 14.0 [48], 13.3 [50]
79	$C_5H_5N^+$	9.6 (0.1)	9.0 [39], 9.25 [49]
80	$^{13}C_5{}^2H_5{}^{15}N^+$	9.2 (0.4)	

Since the major decomposition channels of pyridine have been widely reviewed [27–36], we will omit the discussion of the fragmentation pathways of this molecule. In the present work, we will focus only on unveiling the shake-off dehydrogenation mechanism, which has not been pointed out to our knowledge.

Let us examine the group of peaks formed from the dehydrogenation of the parent ion pyridine ($m/q = 79$). Figure 2 shows the cations generated by sequential abstractions of hydrogens (from one ($m/q = 78$) to five ($m/q = 74$) from the parent ion of pyridine. As seen in Table 1, the appearance energies of peaks with the $m/q = 74$–76 masses are for the first time presented. It can be seen that the

appearance energies rise successively with the number of hydrogens detached, thus suggesting an increasingly complex fragmentation mechanism. The electron generally has insufficient momentum to knock out the atoms from the molecular ring or chain. The molecule may instead tremble after energy deposition due to the ring strain, bending, twisting bonds, and their rupture or formation. Then, the hydrogens may shake off from the cation's closed ring if the newly formed ring molecule has a resonance structure.

Both pyrolysis [54] and photolysis [34] of pyridine start from the C–H bond scission to eliminate hydrogen directly from the closed ring and to produce a $C_5H_4N^+$ pyridyl radical. This radical can be formed in three cyclic *ortho*-, *meta*-, or *para*-pyridyl resonance structures [34]. However, calculations and experiments demonstrated that the *ortho* site's C–H bond cleavage is favored over *m*- and *p*-sites [54]. In our mass spectrum in Fig. 1, the peak $m/q = 78$ corresponding to the pyridyl cation is clearly visible. Its appearance energy is the lowest in that group and agrees with previous determinations.

The following cation ($m/q = 77$) formed from the detachment of two hydrogen atoms is barely visible, even in Fig. 2. Perhaps this is because the other bonds are rearranged in the ring in addition to the second C–H bond breaking. The $C_5H_3N^+$ ($m/q = 77$) may be assigned to the cyclic structure of pyridinediylradical or didehydropyridine or their resonance isomers. The obtained threshold energy value of 15.0 eV is 2.58 eV higher than the literature value. However, our value seems to satisfy the proposed model's conditions better. Indeed, detaching two hydrogen atoms from the ring requires higher energy than detaching one atom (see Table 1).

After the abstraction of another hydrogen, the $C_5H_2N^+$ may remain in a cyclic structure, forming, *e.g.*, pyridine-2,4,6-triylradical ($m/q = 76$). The *o*-pyridyl ring may also open and decompose into several open ring structures with $m/q = 76$ masses. As seen in Table 1, its production requires 1.2 eV more energy than the formation of the $m/q = 77$ cation.

Removing four hydrogen atoms from pyridine may still lead to the formation of the C_5HN^+ in a cyclic ring structure (3,4,5,6-tetradehydropyridine or 2,5-didehydropyridine). It may also rearrange into stable open ring structures. Several different pathways may occur, thus increasing the intensity of this peak ($m/q = 75$) in our spectrum.

The C_5N^+ most likely does not form a stable cyclic structure. Shaking off all hydrogens from the pyridine parent cation does not thus keep the ring closed and must be associated with the ring opening. Even open ring structures are a few. The fragmentation mechanism is somewhat complex and energy-consuming. Therefore, the probability of producing a cation with the $m/q = 74$ mass is low. This fragment starts arising at 29.8 eV.

The peak group with the second-highest masses ($m/q = 60$–64) represents features of the $C_5H_4^+$ molecule's sequential dehydrogenation. The peak intensities in this group diminish with the decrease of the cations' masses, thus suggesting a

lower probability of producing $C_5H_4^+$ ions with fewer attached hydrogen atoms. The probability of fragmentation into these fragments is generally very low because the production of these cations requires, in the first step, isomerization and elimination of the NH radical, which is an unusual fragmentation channel. However, Wasowicz *et al.* [30] showed that hydrogen migration over the pyridine ring in the NH reaction pathway occurs and competes with hydrogen elimination processes. Specifically, they demonstrated that pyridine forms a geometrically stable nonplanar open-ring structure of the $N–H_{ortho}$ tautomer followed by transformation into a five-membered ring of $C_5H_4^+$ with a developed –NH side terminal [30]. The NH detachment can then release an $m/q = 64$ fragment with a ring structure of, for example, 1,2,4-cyclopentatriene. The following fragments in this family can be formed by the successive shaking off of this cyclic structure from subsequent hydrogen atoms. Increasing threshold energies of lower mass cations (Table 1) support this finding.

The cations with masses (m/q = 48-52; 36-39; 24-27) may also arise through this process. However, the lighter the fragment, the more complex pathways can lead to its formation. It is also more difficult for a molecule to form stable structures that can only decompose by shaking. Furthermore, as the previous experimental results show [32], different isobar ions, usually arising *via* diverse fragmentation channels, can represent the same final light fragments. Therefore, quantum-chemical calculations can only unravel a complete course of dehydrogenation of light cations.

4. SUMMARY

We have investigated the dissociative ionization of pyridine, C_5H_5N, molecules in the gas phase by applying electron impact mass spectrometry. It is found that the major cations are the parent, $C_5H_5N^+$, cation (m/q = 79), and the $C_4H_4^+$ fragment (m/q = 52), which have comparable intensities in the 100 eV mass spectra. The E_{TH} of the thirty-two observed cationic fragments have been determined. The E_{TH}'s of sixteen fragments have been found for the first time. Other E_{TH} results generally agree with those determined in the previous ionization experiments.

Analysis shows that some cationic fragments are formed by successive hydrogen atom eliminations. Thus, a new model on the course of a dehydrogenation reaction is proposed here. Such a model mechanism proceeds by sequential hydrogen shake-off from the cation's closed ring structures. It appears accurate for the pyridine parent cation or its fragmentation products, which can form cyclic resonance structures. Indeed, this type of fragmentation is clearly visible in the three heaviest peak groups. However, our description gives a qualitative picture, and quantum-chemical calculations are necessary to get any quantitative data.

Acknowledgments. The EIMS experiment was performed using a quadrupole mass spectrometer at the Laboratory of Complex Systems Spectroscopy of the Gdansk University of Technology

(Fahrenheit Universities' core lab). This article is based upon work from COST Action CA20129 − Multiscale Irradiation and Chemistry Driven Processes and Related Technologies, supported by COST (European Cooperation in Science and Technology).

REFERENCES

1. T.J. Wasowicz, I. Ljubić, A. Kivimäki, R. Richter, Phys. Chem. Chem. Phys. **24**, 19302 (2022).
2. T.J. Wasowicz, A. Kivimäki, D. Catone, R. Richter, Int. J. Mass Spectrom. **449**, 116276 (2020).
3. A. Röder, A. B. Skov, A. E. Boguslavskiy, R. Lausten, A. Stolow, Phys. Chem. Chem. Phys. **22**, 26241 (2020).
4. M. Spanner, S. Patchkovskii, C. Zhou, S. Matsika, M. Kotur, Th. C. Weinacht, Phys. Rev. A **86**, 053406 (2012).
5. T.J. Wasowicz, A. Kivimäki, M. Coreno, M. Zubek, J. Phys. B: At. Mol. Opt. Phys. **45**, 205103 (2012).
6. S. SenGupta, H. P. Upadhyaya, A. Kumar, P. D. Naik, P. Bajaj, J. Chem. Phys. **122**, 124309 (2005).
7. T.J. Wasowicz, A. Kivimäki, M. Dampc, M. Coreno, M. de Simone, M. Zubek, Phys. Rev. A **83**, 033411 (2011).
8. M. Zubek, T. J. Wasowicz, I. Dąbkowska, A. Kivimäki, M. Coreno, J. Chem. Phys. **141**, 064301 (2014).
9. J. A. Trocchi, J. Dech, W. Kedzierski, J. W. McConkey, J. Phys. B At. Mol. Opt. Phys. **52**, 055204 (2019).
10. I. Linert, I. Lachowicz, T. J. Wasowicz, M. Zubek, Chem. Phys. Lett. **498**, 27 (2010).
11. T. J. Wasowicz, I. Linert, I. Lachowicz, M. Zubek, Photonics Lett. Pol. **3**, 110–112 (2011).
12. J. D. Hein, H. Al-Khazraji, C. J. Tiessen, D. Lukic, J. A. Trocchi, J.W. McConkey, J. Phys. B At. Mol. Opt. Phys. **46**, 045202 (2013).
13. T. J. Wasowicz, B. Pranszke, Eur. Phys. J. D **70**, 175 (2016).
14. C. Mejía, G.S. Vignoli Muniz, M. Bender, D. Severin, C. Trautmann, B. Augé, A.N. Agnihotri, P. Boduch, A. Domaracka, H. Rothard, Nucl. Instrum. Methods Phys. Res. B **534**, 11 (2023).
15. T. J. Wasowicz, M. Łabuda, B. Pranszke, Int. J. Mol. Sci. **20**, 6022 (2019).
16. F. Alvarado, S. Bari, R. Hoekstra, T. Schlathöter, Phys. Chem. Chem. Phys. **8**, 1922 (2006).
17. T. J. Wasowicz, Rom. J. Phys. **67**, 206 (2022).
18. Z. Deng, I. Bald, E. Illenberger, M. A. Huels, Phys. Rev. Lett. **95**, 153201 (2005).
19. T. J. Wasowicz, Rom. Rep. Phys. **73**, 203 (2021).
20. T. J. Wasowicz, B. Pranszke, Acta Phys. Pol. A **140**, 228 (2021)
21. T. J. Wasowicz, B. Pranszke, J. Phys. Chem. A **119**, 581–589 (2015).
22. M. Baumann, I. Baxendale, Beilstein J. Org. Chem. **9**, 2265–2319 (2013).
23. P. Kiuru, J. Yli-Kauhaluoma, *Pyridine and Its Derivatives*, in: *Heterocycles in Natural Product Synthesis*, K. Majumdar, S.K. Chattopadhyay (Eds.), Wiley-VCH Verlag GmbH & Co. KgaA, Weinheim, Germany, 2011, pp. 267–297.
24. M. P. Callaghan, K.E. Smith, H.J. Cleaves, J. Ruzicka, J.C. Stern, D.P. Glavin, C.H. House, J.P. Dworkin, Proc. Natl. Acad. Sci. USA **108**, 13995–13999 (2011).
25. K. E. Smith, M.P. Callaghan, P.A. Gerakines, J.P. Dworkin, C.H. House, Geochim. Cosmichim. Acta **136**, 1–12 (2014).
26. D. B. Rap, A. Simon, K. Steenbakkers, J.G.M. Schrauwen, B. Redlich, S. Brünken, Faraday Discuss, 2023, DOI: 10.1039/D3FD00015J.
27. T. J. Wasowicz, Int. J. Mol. Sci. **23**, 205 (2022).
28. P. C. J. A. Bibang, A.N. Agnihotri, P. Boduch, A. Domaracka, Z. Kanuchova, H. Rothard, Eur. Phys. J. D **75**, 57 (2021).
29. T. J. Wasowicz, Res. Phys. **18**, 103244 (2020).

30. T. J. Wasowicz, I. Dabkowska, A. Kivimäki, M. Coreno, M. Zubek, J. Phys. B: At. Mol. Opt. Phys. **50**, 015101 (2017).
31. G. Vall-llosera, M. Coreno, P. Erman, M. A. Huels, K. Jakubowska, A. Kivimäki, E. Rachlew, M. Stankiewicz, Int. J. Mass Spectrom. **275**, 55-63 (2008).
32. C. Q. Jiao, J. C. A. DeJoseph, R. Lee, A. Garscadden, Int. J. Mass Spectrom. **257**, 34 (2006).
33. T. J. Wasowicz, A. Kivimäki, M. Coreno, M. Zubek, J. Phys. B: At. Mol. Opt. Phys. **47**, 055103 (2014).
34. C.-K. Ni, C.-M. Tseng, M.F. Lin, Y.A. Dyakov, J. Phys. Chem. B **111**, 12631–12642 (2007).
35. L. D. Fondren, J. McLain, D. M. Jackson, N. G. Adams, L. M. Babcock, Int. J. Mass Spectrom. **265**, 60−67 (2007).
36. T. J. Wasowicz, B. Pranszke, J. Phys. Chem. A **120**, 964–971 (2016).
37. M. Dampc, I. Linert, M. Zubek, J. Phys. B: At. Mol. Opt. Phys. **48**, 165202 (2015).
38. Pyridine, https://www.sigmaaldrich.com/PL/pl/product/sial/270970 (accessed on March 30, 2023).
39. S. Tixier, G. Cooper, R. Feng, C. E. Brion, J. Elec. Spectrosc. Rel. Phenom. **123**, 185–197 (2002).
40. W. E. Wallace (director), *Mass Spectra* by NIST Mass Spectrometry Data Center in NIST Chemistry WebBook, NIST Standard Reference Database, Number 69, Eds. P.J. Linstrom and W.G. Mallard, National Institute of Standards and Technology, Gaithersburg MD, 20899, https://doi.org/10.18434/T4D303, (retrieved March 31, 2023).
41. M. A. Rahman, E. Krishnakumar, J. Chem. Phys. **144**, 161102 (2016).
42. R. Rejoub, B. G. Lindsay, R. F. Stebbings, Phys. Rev. A **65**, 042713 (2002).
43. D. Hein H. Al-Khazraji, C. J. Tiessen, D. Lukic, J. A. Trocchi, J. W. McConkey, J. Phys. B: At. Mol. Opt. Phys. **46,** 045202 (2013).
44. G. H. Wannier, Phys. Rev. **90**, 817 (1953).
45. M. K. Jurkowski, D. Glowienka, T. J. Wasowicz, Rom. J. Phys. **68**, 203 (2023).
46. M. Jurkowski, D. Glowienka, T. Wasowicz, *ThreSpect a program for the determination of the Appearance Energies* [Data set], Gdansk University of Technology, 2023, https://doi.org/10.34808/hwc6-be20
47. B. Gstir, S. Denifl, G. Hanel, M. Rümmele, T. Fiegele, P. Cicman, M. Stano, S. Matejčik, P. Scheier, K. Becker, A. Stamatovic, T.D. Märk, J. Phys. B: At. Mol. Opt. Phys. **35**, 2993 (2002).
48. J. Momigny, J. Urbain, H. Wankenne, Bull. Soc. R. Sci. Liege **34**, 337 (1965).
49. J.H.D. Eland, J. Berkowitz, H. Schulte, R. Frey, Int. J. Mass Spectrom. Ion Phys. **28**, 297 (1978).
50. B. Jonsson, E. Lindholm, A. Skerbele, Int. J. Mass Spectrom. Ion Phys. **3**, 385 (1969).
51. C. Lifshitz, J. Phys. Chem. **86**, 606 (1982).
52. H. M. Rosenstock, R. Stockbauer, A.C. Parr, Int. J. Mass Spectrom. Ion Phys. **38**, 323 (1981).
53. P. C. Burgers, J.L. Holmes, Int. J. Mass Spectrom. Ion Proc. **58**, 15 (1984).
54. J. H. Kiefer, Q. Zhang, R. D. Kern, J. Yao, B. Jursic, J. Phys. Chem. A **101**, 7061–7073 (1997).